

This is the accepted manuscript made available via CHORUS. The article has been published as:

## Effects of surfactant transport on electrodeformation of a viscous drop

Herve Nganguia, On Shun Pak, and Y.-N. Young

Phys. Rev. E **99**, 063104 — Published 10 June 2019

DOI: [10.1103/PhysRevE.99.063104](https://doi.org/10.1103/PhysRevE.99.063104)

# Effects of surfactant transport on electrodeformation of a viscous drop

Herve Nganguia

*Department of Mathematical and Computer Sciences,  
Indiana University of Pennsylvania, Indiana, Pennsylvania 15705, USA*

On Shun Pak

*Department of Mechanical Engineering, Santa Clara University, Santa Clara, California 95053, USA*

Y.-N. Young\*

*Department of Mathematical Sciences, New Jersey Institute of Technology, Newark, New Jersey 07102, USA*

(Dated: May 17, 2019)

In this work we quantify the effects of surfactant transport on the deformation of a viscous drop under a DC electric field. We study how convective and diffusive transport of surfactants at drop surfaces influence the equilibrium and dynamic deformation of a leaky dielectric drop and a conducting drop. Focusing on the prolate drop shape (elongates along the electric field), we show the differences in equilibrium deformation and flow circulation between a leaky dielectric drop and a conducting drop. We quantify the drop electrodeformation via its dependence on the interior flow circulation and the dominant surfactant transport regime (characterized by the surface Péclet number  $Pe_s$ ). For a leaky dielectric drop with dominant surfactant diffusion ( $Pe_s \ll 1$ ), equator-to-pole (pole-to-equator) circulation yields smaller (larger) equilibrium deformation with increasing surfactant coverage, compared to a clean drop. On the other hand, when convection dominates ( $Pe_s \gg 1$ ), the equilibrium drop deformation increases (decreases) with larger surfactant coverage for equator-to-pole (pole-to-equator) circulation. Larger equilibrium drop deformation is found for a leaky dielectric drop than a conducting drop when the interior flow is from equator to pole. For an interior flow from pole to equator, we identify cases where larger deformation is found for a conducting interior fluid. Finally, we study the effect of the surfactant transport on the dynamic evolution of drop shape. We found the drop undergoes an overshoot in the early deformation phase, before settling to its equilibrium shape –similar to the overshoot observed for unsteady Stokes flow.

---

\* Corresponding author: [yyoung@njit.edu](mailto:yyoung@njit.edu)

## I. INTRODUCTION

Electric field is widely utilized to deform a viscous drop in microfluidics and many petroleum engineering applications. For a leaky dielectric drop freely suspended in another leaky dielectric fluid, the bulk charge neutralizes on a fast time scale while free charges accumulate on the drop surface under an electric field. Analytical investigation of the electro-deformation of a viscous drop has been conducted [1, 2], and the electrohydrodynamic (EHD) leaky dielectric model [3] has been developed to explain the deformation of conducting drops suspended in a conducting medium. Results show that the electrostatic stresses on the drop surface lead to interior toroidal circulations. Consequently the drop deforms to either a prolate or an oblate spheroid shape depending on the specific electrical properties of fluids [4]. With different electrical properties the effects of the electrostatic and hydrodynamic stresses on drop deformation also behaves distinctively [5]. Under a small electric field, a steady equilibrium drop shape exists due to the balance between the electric and hydrodynamic stresses [6–8]. Under a sufficiently large electric field, no steady equilibrium drop shape is stable and the drop keeps deforming until the eventual break-up into smaller drops [9, 10].

Analytical treatments of the electro-deformation in the leaky dielectric framework assume either small deformations or specific spheroidal (oblate or prolate) shapes. These results predict the dependence of the equilibrium drop shape on the electric capillary number (ratio of electric stress to surface tension). Such dependence was first derived by Taylor [3] for small deformation of a spherical drop in a weak uniform electric field. A comprehensive review of the theoretical developments in this area can be found in Melcher and Taylor [4] and Saville [5]. Benteritis and Krause [11] extended Taylor’s leaky dielectric model for large deformation of a non-charged viscous drop in a dielectric fluid by a strong electric field. Their large deformation analysis assumes spheroidal shapes and gives reasonable agreement with most experiments for the prolate drops, while discrepancies are observed for oblate drops. Zabaranin reformulated the stress boundary condition on a spheroidal drop and used a non-Stokes stream function to calculate the steady flow around a spheroidal drop under a DC electric field [12, 13]. In this new formulation Zabaranin predicted large steady prolate spheroidal drop deformation consistent with results from both experiments and previous spheroidal models.

Direct numerical simulations of an axisymmetric or two-dimensional drop in an electric field have been conducted to investigate strong electro-deformation in the framework of the leaky dielectric model [8, 14–19]. Under strong electric forces conical points may form at the end of the viscous drop [20], from where small drops may be streaming as a result of the instability (tip streaming). The viscous drop may also undergo large deformation with undulation, and eventually break up into several drops of comparable sizes. While both phenomena require special numerical treatment to capture the topological changes due to the instability, tip streaming requires numerical resolution for the structures and dynamics at the conical points [15, 16].

Recent studies have reported the effects of charge relaxation and convection on the dynamics of drop deformation within the leaky dielectric framework [21–23]. In the absence of charge convection, relaxation affects the transient dynamic of the prolate (oblate) drop by causing a short-lived shape transition at the early phase of drop evolution, but it does not alter the equilibrium deformation. On the other hand, without relaxation, charge convection gives rise to monotonic deformation dynamics that asymptotes to an equilibrium with shape-dependent differences: Equilibrium deformation is enhanced for a prolate drop [24], and reduced for an oblate drop (completely stabilized for an otherwise unstable oblate drop) [22]. Lanauze *et al.* [21] also considered inertial effects by solving the unsteady Stokes equation. They show inertia leads to an overshoot in the transient evolution of the drop at the later phase of the dynamic prior to reaching equilibrium; this result is consistent with existing numerical simulations [8, 25].

Surfactants are extensively used to reduce drop size by lowering surface tension in many engineering applications that involve drop deformation and breakup [26, 27]. Surface tension reduction by surfactant can substantially alter interfacial evolution and the flow: A striking example is the surfactant-induced tip streaming of small drops from a thin viscous thread extended from a bubble deformed by an imposed shear or strain [28]. Experiments and analyses show that surfactant has a significant effect on the stability of a viscous jet surrounded by another viscous fluid. Linear stability of a surfactant-laden cylindrical jet shows that surfactant affects the growth rate of disturbances via a combination of reduced surface tension and the immobilizing (surface stiffening) effect of the Marangoni stress. The equilibrium electro-deformation of a surfactant-laden viscous drop has been investigated experimentally by Ha and Yang [29, 30] (small-deformation analysis and experiments), and later numerically by Teigen and Munkejord [31] (axisymmetric numerical simulations) and semi-analytically by Nganguia *et al.* [32] (large deformation analysis). While Ha and Yang concluded that surfactant leads to enhanced electro-deformation for a prolate drop, Teigen and Munkejord found that smaller deformation may be caused by surfactant if the surfactant concentration is small, leading to an opposite circulation inside the viscous drop. These phenomena have been captured and explained by an analytical spheroidal model for a surfactant-laden viscous drop in the limit of weak surfactant diffusivity [32].

The Marangoni stress depends on the surfactant transport characterized by the surface Péclet number  $Pe_s$ , the ratio of convective to diffusive transport. To our knowledge, studies on the effects of surfactants on the deformation of drops subject to electric fields [31, 32] have focused on transport dominated by convection, where  $Pe_s \gg 1$ .

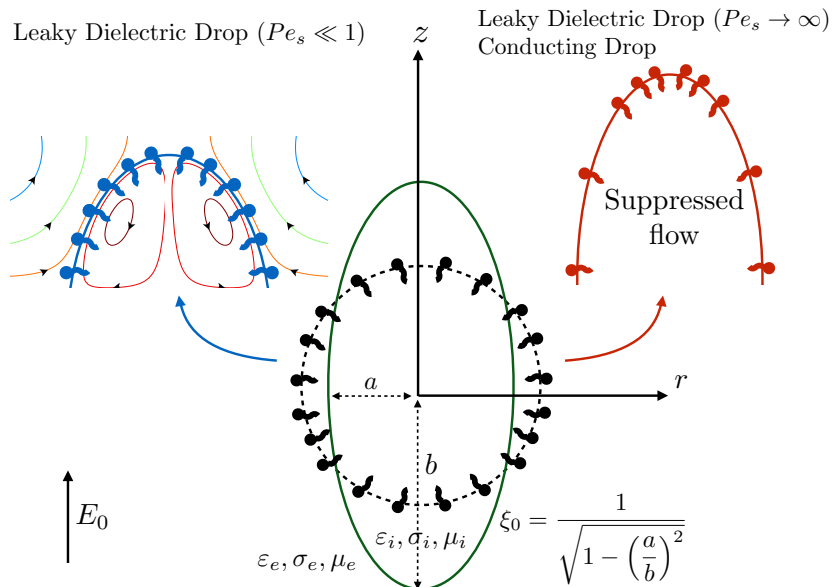


FIG. 1. A viscous drop, subject to a DC electric field  $E_0 \mathbf{e}_z$  and covered with insoluble surfactant (bead-rod particles), separates two immiscible fluids, with physical parameters  $\varepsilon_j, \sigma_j, \mu_j$ , where  $j = i$  denotes the interior of the drop, and  $j = e$  its exterior. Application of the electric field induces flow inside and outside the drop which deforms into a prolate-shaped spheroid at equilibrium. Deformation depends on the type of drops (leaky dielectric or conducting), and on the surfactant transport mechanism (diffusive transport for  $Pe_s \ll 1$  and convective transport for  $Pe_s \rightarrow \infty$ ). The drop shape parameter  $\xi_0$  is a function of the aspect ratio between the major ( $b$ ) and minor ( $a$ ) axes.

While these studies have enhanced our understanding of the combined effects of electric fields and surfactants on the electrohydrodynamics of drops, the influence of diffusive surfactant transport on equilibrium deformation, and on the transient evolution of drops remain unexplored. Here we investigate the effects of surfactants on drop electro-deformation from diffusion-dominant to moderate convective transport ( $Pe_s \leq 10$ ). To this end, we present a semi-analytical method to simulate drops electrohydrodynamics over a range of surface Péclet numbers.

The paper is organized as follows. In §II we first formulate the leaky dielectric model. We then present the analytical solution in the spheroidal coordinates (§II A 1), and the resulting shape equation for surfactant-laden drops (§II A 2). Finally, we introduce the modified equations for a conducting drop (§II B), before discussing the dependence of surface tension on surfactant concentration in §II C. In §III we validate our spheroidal model against experimental data for a clean conducting drop (§III A), and against numerical simulations for a leaky dielectric, surfactant-laden drop (§III B). We then utilize the model to analyze the effects of surfactant transport on the equilibrium deformation of leaky dielectric and conducting drops (§IV), and on the transient dynamic (§V). Finally in §VI we draw conclusion on our findings and discuss future research direction.

## II. PROBLEM FORMULATION

### A. Leaky dielectric drops

We consider a viscous drop immersed in a leaky dielectric fluid as shown in figure 1. Each fluid is characterized by the fluid viscosity  $\mu$ , dielectric permittivity  $\varepsilon$ , and conductivity  $\sigma$  with the subscript denoting interior (i) or exterior (e) fluid. In this work the subscript “r” denotes the ratio between exterior and interior quantities:  $\mu_r = \mu_e/\mu_i$ ,  $\varepsilon_r = \varepsilon_e/\varepsilon_i$ , and  $\sigma_r = \sigma_e/\sigma_i$ . Typical applications of leaky dielectric fluids involve drops of mm size under an electric field strength of kV/cm. Hence we can safely assume that the fluid flow in this system is in the creeping flow regime with negligible inertia.

The interior and exterior fluids are governed by the incompressible Stokes equations

$$\mu_j \nabla^2 \mathbf{u}_j = \nabla p_j, \quad (1)$$

$$\nabla \cdot \mathbf{u}_j = 0, \quad (2)$$

where the subscript  $j$  denotes interior ( $j = i$ ) or exterior ( $j = e$ ) fluids. In the far-field the flow is quiescent,

$$\mathbf{u}_e(\mathbf{x} \rightarrow \infty) = \mathbf{0}. \quad (3)$$

The drop shape evolves according to

$$\frac{\partial \mathbf{X}}{\partial t} = v \mathbf{n}, \quad (4)$$

where  $\mathbf{X}$  is a point on the drop surface and  $v = \mathbf{u} \cdot \mathbf{n}$  is the interfacial velocity along the normal direction  $\mathbf{n}$ .

The stress balance at the drop surface gives

$$\llbracket (\mathbf{T}^H + \mathbf{T}^E) \cdot \mathbf{n} \rrbracket = \gamma (\nabla \cdot \mathbf{n}) \mathbf{n} - \nabla_s \gamma \cdot \mathbf{t}, \quad (5)$$

where  $\llbracket f \rrbracket \equiv f_e - f_i$  denotes the difference across the drop surface;  $\gamma$  is the surface tension that depends on the surfactant distribution on the surface;  $\mathbf{t}$  and  $\mathbf{n}$  are the unit tangential and normal vectors, respectively, on the drop surface; the hydrodynamic stress  $\mathbf{T}^H = -p\mathbf{I} + \mu [(\nabla \mathbf{u})^T + \nabla \mathbf{u}]$ , and the Maxwell stress  $\mathbf{T}^E = \varepsilon \mathbf{E} \mathbf{E} - \frac{1}{2} \varepsilon (\mathbf{E} \cdot \mathbf{E}) \mathbf{I}$ , with  $\varepsilon$  the permittivity of the fluid. We can write the Maxwell stress for a leaky dielectric drop in terms of the permittivity and conductivity ratios,

$$\llbracket \mathbf{T}^E \rrbracket = \varepsilon_e \left\{ \frac{1}{2} \left[ E_n^2 \left( 1 - \frac{\sigma_r^2}{\varepsilon_r} \right) - E_t^2 \right] \mathbf{n} + E_n E_t \left( 1 - \frac{\sigma_r}{\varepsilon_r} \right) \mathbf{t} \right\}. \quad (6)$$

The electric field  $\mathbf{E} = -\nabla \phi$ , where  $\phi$  is the electric potential that satisfies the Laplace equation both inside and outside the drop in the extended leaky dielectric model

$$\nabla^2 \phi_j = 0. \quad (7)$$

Far away from the drop surface the electric field is the imposed electric field

$$-\nabla \phi_e = E_0 \mathbf{z}. \quad (8)$$

At the drop surface the tangential electric field is continuous while the normal electric field has a jump due to the displacement current:

$$\llbracket \nabla \phi \cdot \mathbf{t} \rrbracket = 0, \quad \llbracket \sigma \nabla \phi \cdot \mathbf{n} \rrbracket = \frac{\partial q}{\partial t}, \quad (9)$$

where  $q \equiv \llbracket -\varepsilon \nabla \phi \cdot \mathbf{n} \rrbracket$  is the surface charge density with  $\sigma$  the conductivity of the fluid. While charge relaxation ( $\partial q / \partial t$ ) may be significant for large drops (such as mm sized Tween-laden drops in silicone oil), here we assume that charge relaxation is negligible ( $\partial q / \partial t \approx 0$ ) for smaller drops as a first approximation. In this case, the conservation of current Eq. 9 reduces to the continuity of Ohmic current,  $\llbracket \sigma \nabla \phi \cdot \mathbf{n} \rrbracket = 0$ .

The surfactant transport on the drop surface in the Lagrangian framework is described by the following equation

$$\frac{\partial \Gamma}{\partial t} + \nabla_s \cdot (\mathbf{u}_s \Gamma) + \kappa \mathbf{u} \cdot \mathbf{n} \Gamma = D_s \nabla_s^2 \Gamma, \quad (10)$$

where  $\Gamma$  is the surfactant concentration,  $\nabla_s \equiv (\mathbf{I} - \mathbf{n} \mathbf{n}) \cdot \nabla$  is the gradient projected on the drop surface,  $\mathbf{u}_s \equiv (\mathbf{I} - \mathbf{n} \mathbf{n}) \cdot \mathbf{u}$  is the tangential velocity on the surface,  $\kappa$  is the mean curvature, and  $D_s$  is the diffusion constant of the surfactant on the drop surface.

### 1. Analytical solution

The spheroidal coordinates system has been used successfully to analyze the electrohydrodynamics of clean [11, 33, 34] and surfactant-laden [32] leaky dielectric drops. The large deformation analysis, to contrast with the oft-used small-deformation theory, rests on assumptions that naturally constrain its validity. We expand on these limitations in Appendix B 1. However we note that in the case of surfactant-laden drops, provided the drop remains spheroidal, our model agrees well with experimental and numerical data for moderate and large Péclet numbers [35]. Here we only provide a general outline of the method used to derive the shape equation §II A 2. Focusing on the axisymmetric flow, the prolate spheroidal coordinates  $(\xi, \eta)$  can be expressed in the cylindrical coordinates  $(r, z)$  as

$$z = c \xi \eta, \quad r = c \sqrt{(\xi^2 - 1)(1 - \eta^2)}, \quad (11)$$

with  $c \equiv \sqrt{a^2 - b^2}$  is the semi-focal length, and  $a$  and  $b$  are the major and minor semi-axis, respectively. Defined as such,  $\xi \in [1, \infty)$ ,  $\eta \in [-1, 1]$ , and surfaces of constant  $\xi$  are spheroids while surfaces of constant  $\eta$  are hyperboloids. Therefore the prolate drop surface is simply given by  $\xi = \xi_0(t) \equiv a/c$ . Volume conservation of the drop relates  $a$  and  $b$  to  $\xi_0(t)$  as  $a(t) = r_0 / \sqrt[3]{1 - \xi_0(t)^{-2}}$  and  $b(t) = r_0 \sqrt[3]{1 - \xi_0(t)^{-2}}$ . In the following we use  $h_\xi$ ,  $h_\eta$  and  $h_\zeta$  to denote the metric coefficients in the prolate spheroidal coordinates. The hydrodynamic and electric potential problems can be solved separately. The potential  $\phi$  is obtained by solving Eq. 7 for both  $\phi_i$  and  $\phi_e$  with boundary and matching conditions at the drop surface [34]:

$$\phi_e = [-E_0 c \xi + \alpha(t) Q_1(\xi)] \eta, \quad (12)$$

$$\phi_i = \beta(t) \xi \eta, \quad (13)$$

with

$$\alpha(t) = \frac{\xi_0 \beta(t) + E_0 c \xi_0}{Q_1(\xi_0)}, \quad (14)$$

and  $Q_1(\xi)$  the first-degree Legendre polynomial of the second kind. In the absence of charge relaxation, the boundary condition in the normal direction given by Eq. 9 reduces to the widely used interfacial boundary condition

$$\llbracket \sigma \nabla \phi \rrbracket = \sigma_e \frac{\partial \phi_e}{\partial \xi} - \sigma_i \frac{\partial \phi_i}{\partial \xi} = 0 \text{ at } \xi = \xi_0. \quad (15)$$

With this simplified interfacial condition, the electric potential coefficients,  $\alpha(t)$ ,  $\beta(t)$  are given by

$$\alpha(t) = \frac{c \xi_0 (\sigma_r - 1)}{\xi_0 \sigma_r Q'_1 - Q_1}, \quad \beta(t) = \frac{c \sigma_r (Q_1 - \xi_0 Q'_1)}{\xi_0 \sigma_r Q'_1 - Q_1}, \quad (16)$$

where the primes denote derivatives with respect to  $\xi$ .

Next we focus on the hydrodynamic problem. The axisymmetric two-dimensional incompressible fluid velocity is related to a stream function  $\psi$  both inside and outside the drop via

$$u_j = -\frac{1}{h_\xi h_\zeta} \frac{\partial \psi_j}{\partial \xi}, \quad v_j = \frac{1}{h_\eta h_\zeta} \frac{\partial \psi_j}{\partial \eta}, \quad (17)$$

where  $u$  and  $v$  are the tangential and normal components (relative to the drop surface) of the fluid velocity. The stream function satisfies the equation

$$(\nabla^2)^2 \psi = 0, \quad (18)$$

with

$$\nabla^2 = \frac{1}{c^2(\xi^2 - \eta^2)} \left[ \frac{\partial}{\partial \xi} (\xi^2 - 1) \frac{\partial}{\partial \xi} + \frac{\partial}{\partial \eta} (1 - \eta^2) \frac{\partial}{\partial \eta} \right].$$

The general solution to Eq. 18 can be expressed using the method of semi-decomposition

$$\psi = g_0(\xi) G_0(\eta) + g_1(\xi) G_1(\eta) + \sum_{n=2}^{\infty} g_n(\xi) G_n(\eta) + h_n(\xi) H_n(\eta), \quad (19)$$

where  $G_n$  and  $H_n$  are Gegenbauer functions of the first and second kinds, respectively.  $g_n$  and  $h_n$  are linear combinations of  $G_n$  and  $H_n$ . Interested readers are referred to Dassios *et al.* [36] for detailed expressions of  $G_n$ ,  $H_n$ ,  $g_n$  and  $h_n$ . Following the approaches in Bentein and Krause [11] and Zhang *et al.* [34], we seek an approximate solution

$$\psi_e = [A_3^1 H_1(\xi) + A_3^3 H_3(\xi)] G_3(\eta), \quad (20)$$

$$\psi_i = [B_3^3 G_3(\xi) + B_3^5 G_5(\xi)] G_3(\eta). \quad (21)$$

The tangential velocity is continuous across the drop surface and has to be determined consistently through the stress balance, while the normal component of the interface velocity can be computed explicitly as

$$v(\xi_0) = \frac{r_0(1 - \xi_0^{-2})^{-5/6}}{3\xi_0^2} \frac{(1 - 3\eta^2)}{\sqrt{\xi_0^2 - \eta^2}} \frac{d\xi_0}{dt}.$$

The coefficients  $A_3^1$ ,  $B_3^3$ , and  $B_3^5$  are determined from the continuity of velocities at the drop surface together with the kinematic condition  $\mathbf{u} \cdot \mathbf{n} = v(\xi_0)$ . The remaining coefficient  $A_3^3$  and the rate of deformation of drop shape  $d\xi_0/dt$  are computed from the stress balance equation (Eq. 6) averaged over the drop surface in the energetic fashion as done by Zhang *et al.* [34]. In spheroidal coordinates, the tangential and normal components of the averaged stress, respectively, are

$$\int_{\xi=\xi_0(t)} u \left[ \llbracket T_{\xi\eta}^H \rrbracket + \llbracket T_{\xi\eta}^E \rrbracket + \frac{1}{h_\eta} \frac{\partial \gamma}{\partial \eta} \right] ds = 0, \quad (22)$$

$$\int_{\xi=\xi_0(t)} v \left[ \llbracket T_{\xi\xi}^H \rrbracket + \llbracket T_{\xi\xi}^E \rrbracket - \gamma (\nabla \cdot \mathbf{n}) \right] ds = 0. \quad (23)$$

It is straightforward to show  $A_3^1 = A_3^3 H_3 - M d\xi_0/dt$ ,  $B_3^3 = (-A_3^3 G_5 H_3' + M G_5' d\xi_0/dt)/N$ , and  $B_3^5 = (A_3^3 G_3 H_3' - M G_3' d\xi_0/dt)/N$ , where  $M = 2c^3/3$  and  $N = G_3 G_5' - G_5 G_3'$ . At steady state ( $d\xi_0/dt = 0$ ), all coefficients in Eqs. 20 and 21 can be expressed in terms of  $A_3^3$ , which therefore represents the strength of the flow field inside and outside the drop.

## 2. Shape equation

We non-dimensionalize lengths using the drop radius  $r_0$ , and time using the EHD flow time scale  $\tau_{EHD} = r_0/U$ , where  $U$  is a characteristic velocity. The electric potential is scaled using  $E_0 r_0$ , and surface tension using  $\gamma^*$  of the convection-free case. In terms of the variables we have  $\alpha = E_0 r_0 \tilde{\alpha}$ ,  $\beta = E_0 r_0 \tilde{\beta}$ , and  $c = r_0 \tilde{c}$ . Hereafter we drop the tildes for simplicity and refer to only dimensionless quantities unless otherwise stated.

The coefficient  $A_3^3$  is determined from the stress balance as

$$A_3^3 = \frac{-Ca_E c^3 \mathcal{Q}_T \xi_0 f_{11} + \mathcal{E} c^2 f_{17} - Ca_E [(\mu_r - 1) f_{12} + f_{13}] M \frac{d\xi_0}{dt}}{-(\mu_r f_{14} + f_{15})}, \quad (24)$$

where  $Ca_E = E_0^2 r_0 \varepsilon_e / \gamma^*$  is the electric capillary number,  $\mathcal{E} = E\chi/[1 + E \ln(1 - \chi)]$ , and the elasticity number  $E = RT\Gamma_\infty/\gamma_0$  is a measure of the sensitivity of surface tension to changes in the concentration of adsorbed surfactant on the drop surface, expressed in terms of the gas constant  $R$ , temperature  $T$  and the surface tension of a clean drop  $\gamma_0$ . The system is closed with the evolution equation for the prolate drop shape  $\xi_0$

$$\frac{d\xi_0}{dt} = \frac{3}{2} \frac{f_{\mathcal{Q}_N} + f_{\mathcal{Q}_T} + f_{Ma} + f_\gamma}{(\mu_r f_{25} + f_{26})}, \quad (25)$$

where

$$f_{\mathcal{Q}_N} = \mathcal{Q}_N f_{21}, \quad (26a)$$

$$f_{\mathcal{Q}_T} = \mathcal{Q}_T \frac{\xi_0 f_{11} (\mu_r f_{22} + f_{23})}{\mu_r f_{14} + f_{15}}, \quad (26b)$$

$$f_{Ma} = -\frac{E\chi}{Ca_E c [1 + E \ln(1 - \chi)]} \frac{f_{17} (\mu_r f_{22} + f_{23})}{\mu_r f_{14} + f_{15}}, \quad (26c)$$

$$f_\gamma = -\frac{f_{24}}{Ca_E}, \quad (26d)$$

$$\mathcal{Q}_N = \frac{1}{c^2} \left[ (-c + \alpha(t) Q_1')^2 + \left( -c + \alpha(t) \frac{Q_1}{\xi_0} \right)^2 - 2 \frac{\beta^2(t)}{\varepsilon_r} \right], \quad (26e)$$

$$\mathcal{Q}_T = \frac{1}{c^2} \left[ (-c + \alpha(t) Q_1') (-c + \alpha(t) \frac{Q_1}{\xi_0}) - \frac{\beta^2(t)}{\varepsilon_r} \right]. \quad (26f)$$

$f_{\mathcal{Q}_N}$ ,  $f_{\mathcal{Q}_T}$ ,  $f_{Ma}$  and  $f_\gamma$  represent, respectively, the contributions of the Maxwell stresses, Marangoni stress and surface tension to the shape of the drop. The shape-dependent functions  $f_{11}$ ,  $f_{12}$ ,  $f_{13}$ ,  $f_{14}$ ,  $f_{15}$ ,  $f_{17}$ ,  $f_{21}$ ,  $f_{22}$ ,  $f_{23}$ ,  $f_{24}$ ,  $f_{25}$ , and  $f_{26}$  are provided in Appendix A. In the absence of charge relaxation, contributions from the Maxwell stresses  $f_{\mathcal{Q}_N}$  given by Eq. 26a and  $f_{\mathcal{Q}_T}$  given by Eq. 26b reduce to

$$f_{\mathcal{Q}_N} = -K^2 \left( 2 \frac{\sigma_r^2}{\varepsilon_r} - \sigma_r^2 - 1 \right) f_{21}, \quad f_{\mathcal{Q}_T} = K^2 \sigma_r \left( 1 - \frac{\sigma_r}{\varepsilon_r} \right) \frac{\xi_0 f_{11} (\mu_r f_{22} + f_{23})}{\mu_r f_{14} + f_{15}}, \quad (27)$$

where  $K \equiv [Q_1(\xi_0) - \xi_0 Q_1'(\xi_0)] / [Q_1(\xi_0) - \sigma_r \xi_0 Q_1'(\xi_0)]$ .

## B. Conducting drops

For a conducting drop the conductivity ratio  $\sigma_r \ll 1$ , and consequently there is no tangential electric field on the interface ( $E_t = \mathbf{E} \cdot \mathbf{t} \rightarrow 0$ ) [33, 37, 38]. The general formulation for the bulk follows that of leaky dielectric drops: the fluids in the exterior and interior are governed by the incompressible Stokes Eq. 1-2 with prescribed far-field and kinematic boundary conditions. The main difference is in the boundary conditions that are related to the Maxwell stress  $\mathbf{T}^E$ : For a conducting drop, Eq. 6 reduces to

$$\llbracket \mathbf{T}^E \rrbracket = \frac{\varepsilon_e}{2} E_n^2 \mathbf{n}. \quad (28)$$

In terms of spheroidal coordinates for a conducting drop, Eq. 22 reduces to

$$\int_{\xi=\xi_0(t)} u \left( \llbracket T_{\xi\eta}^H \rrbracket + \frac{1}{h_\eta} \frac{\partial \gamma}{\partial \eta} \right) ds = 0. \quad (29)$$

In the absence of tangential electric stresses, Eq. 29 informs us that the hydrodynamic flow is instead balanced by Marangoni stresses. In this case the velocity  $U$  scales as  $\gamma^*/\mu_e$ , giving  $t = \tau_\gamma \tilde{t}$  where  $\tau_\gamma = r_0 \mu_e \gamma^*$  is the hydrodynamic time scale. We obtain the flow strength

$$A_3^3 = \frac{\mathcal{E} c^2 f_{17} - [(\mu_r - 1) f_{12} + f_{13}] M \frac{d\xi_0}{dt}}{-(\mu_r f_{14} + f_{15})}, \quad (30)$$

and the shape equation

$$\frac{d\xi_0}{dt} = \frac{3}{2} \frac{f_{\mathcal{Q}_N} + f_{Ma} + f_\gamma}{(\mu_r f_{25} + f_{26})}, \quad (31)$$

where  $f_{\mathcal{Q}_T} = 0$  and  $f_{\mathcal{Q}_N}$  now takes the form

$$f_{\mathcal{Q}_N} = \frac{Ca_E}{c^2} \left[ (-c + \alpha(t) Q_1')^2 - 2 \frac{\beta^2(t)}{\varepsilon_r} \right] f_{21}. \quad (32)$$

## C. Surface tension and surfactant transport

We adopt the Langmuir equation of state for the surface tension  $\gamma$  of the surfactant-laden drop surface

$$\gamma = \gamma_0 [1 + E \ln(1 - \Gamma)]. \quad (33)$$

The Langmuir equation of state is not valid for surfactant concentration above the maximum packing concentration, beyond which the integrity of the surfactant monolayer is compromised by micelle formation. This is often observed during tip streaming [39–41] and thread formation [42, 43]. Here, we only consider equilibrium drop shape for low to moderate surfactant concentration, below the maximum packing concentration.

The equation for the surfactant concentration is non-dimensionalized by scaling the surfactant by  $\Gamma = \Gamma^* \tilde{\Gamma}$ , where  $\Gamma^*$  is the surfactant distribution in the convection-free case ( $D_s \rightarrow \infty$ ), and the surface tension  $\gamma = \gamma^* \tilde{\gamma}$ , where  $\gamma^* = \gamma_0 [1 + E \ln(1 - \chi)]$ . Again dropping the tildes, the equation of state becomes

$$\gamma(\Gamma) = \frac{1 + E \ln(1 - \chi \Gamma)}{1 + E \ln(1 - \chi)}, \quad (34)$$

where  $\chi = \Gamma^*/\Gamma_\infty$  is the surfactant coverage.

The dimensionless surfactant transport equation

$$Pe_s \left[ \frac{\partial \Gamma}{\partial t} + \nabla_s \cdot (\Gamma \mathbf{u}_s) + (\mathbf{u} \cdot \mathbf{n}) \kappa \Gamma \right] = \nabla_s^2 \Gamma, \quad (35)$$

where  $Pe_s = U r_0 / D_s$  is the dimensionless Péclet number (a measure of the relative importance of convective transport to diffusive transport), and  $U$  is a characteristic velocity.



For electrically driven flow  $U$  scales as  $\varepsilon_e E_0^2 r_0 / \mu$ , and the Péclet number is proportional to the square of the electric field strength. We can then estimate the Péclet number by considering typical values for a Tween-laden drop in silicone oil. The oil phase has viscosity  $\mu \approx 10$  Pa·s and dielectric constant  $\varepsilon_e / \varepsilon_0 = 2.2 - 2.9$ , where  $\varepsilon_0$  is the vacuum permittivity [44]. In experiments [2, 44–46], typical values of the electric field are in the order of kV/cm. For a drop of size one millimeter [45], the velocity  $U$  is estimated of order  $10^{-3}$  mm/s. With surfactant diffusivity  $D_s \approx 10^{-10}$  m<sup>2</sup>/s [47], we obtain Péclet number of order 10. For smaller drops with size of order tens of microns [2, 46], the Péclet number could be as small as  $10^{-3}$ . Thus we can expect diffusive transport to contribute significantly to the dynamics.

In the axisymmetric spheroidal coordinates, Eq. 35 takes the following form

$$Pe_s \left[ \frac{\partial \Gamma}{\partial t} + \frac{u}{h_\eta} \frac{\partial \Gamma}{\partial \eta} + \left( \frac{1}{h_\eta} \frac{\partial u}{\partial \eta} + \kappa v \right) \Gamma \right] = \frac{1}{h_\eta} \frac{\partial}{\partial \eta} \left( \frac{1}{h_\eta} \frac{\partial \Gamma}{\partial \eta} \right). \quad (36)$$

The large deformation spheroidal analysis provides an efficient tool to determine the drop shape and the corresponding flow field compared to direct numerical simulations of the full system. The nonlinear surfactant transport equation (Eq. 36) however may not be tractable analytically except for some asymptotic limits in Péclet number. To investigate the dynamics for a range of intermediate Péclet number, we develop a hybrid, semi-analytical approach to solve the full set of equations. The spheroidal representation of the drop shape is combined with a numerical collocation method for determining the surfactant concentration profile on the spheroidal surface. Details of the numerical implementation can be found in Appendix B 2.

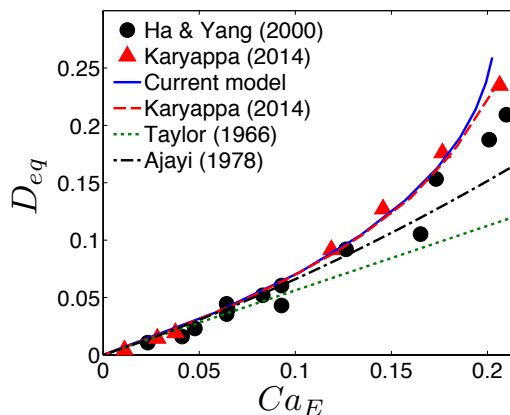


FIG. 2. Equilibrium deformation  $D_{eq}$  as a function of electric capillary number for a clean conducting drop. The parameters  $\mu_r = 1/0.00126$ ,  $\sigma_r = 10^{-8}$ ,  $\varepsilon_r = 1/31.1$ . The symbols denote experiments [6, 48]; the curves represent predictions using the boundary integral method (dashed) [48], Taylor’s first order theory (dotted), and Ajayi’s second order approximation (dash-dotted). The present model is shown in solid line.

### III. MODEL VALIDATION

Conducting drops can only achieve prolate shapes at equilibrium due to the absence of electric field-induced tangential flows. Since our main focus is to contrast the effects of surfactant transport on leaky dielectric versus conducting drops, extension to oblate shapes is beyond the scope of this paper and is deferred to future studies. Furthermore we consider identical viscosity between the continuous phase and the drop ( $\mu_r = 1$ ), and the surfactant elasticity  $E = 0.2$ . We characterize drop deformation via the deformation number  $D \equiv (a - b)/(a + b)$ .

#### A. Equilibrium deformation of clean conducting drop

The large deformation analysis of a viscous drop has garnered increasing interest in recent years. In the absence of surfactants (the surface tension  $\gamma$  is a constant and  $f_{Ma} = 0$  in Eq. 31), large-deformation studies have shown excellent agreements with both numerical simulations [10] and experiments [6] for a leaky dielectric drop under a DC electric field. The main reason for the growing popularity of the large-deformation analysis is that without too much

more work than the small-deformation analysis, the spheroidal model for a clean drop in a DC field gives excellent agreement with experimental data over a wide range of capillary number and deformation as long as the drop shape remains spheroidal (see appendix in [32]).

Here we show the accuracy of the large-deformation analysis for the case of clean spheroidal conducting drops. At the steady equilibrium  $d\xi_0/dt = 0$  in Eq. 31, giving  $\mathcal{Q}_N f_{21} = f_{24}$ , where  $\mathcal{Q}_N$  is given by Eq. 26e. This equation is nonlinear in the drop shape coordinate  $\xi_0$ . Alternatively, we can consider the inverse problem of determining the electric capillary number  $Ca_E$  for a given drop shape  $\xi_0$ . Figure 2 shows the comparison between the results obtained from solving for  $\xi_0$  from Eq. III A and numerical simulations [48] and experiments (triangle and circle symbols) [6, 48] of electrohydrodynamics of a conducting drop. We also plot results for the first- [3] and second-order [49] small-deformation theory. At small values of the electric capillary number ( $Ca_E \leq 0.1$ ) all analytical and numerical models are in excellent agreement with the experimental data. The first-order small deformation approximation underestimates the equilibrium drop deformation around  $Ca_E \approx 0.1$ , while predictions from the second-order small deformation model hold up to  $Ca_E \approx 0.15$ . For this problem, the spheroidal model captures the full range of experimental observations as well as numerical simulations.

### B. Effects of surfactant coverage on drops deformation

In this section, and in the rest of the analysis, we focus our attention on two distinct modes of deformation: prolate ‘A’ drop that exhibits counter-clockwise (equator to pole) circulation; and prolate ‘B’ drop with clockwise circulation (pole to equator). For comparison we use the same values for the dimensionless parameters as in [31]:  $\varepsilon_r = 1, \sigma_r = 1/3$  for prolate ‘A’, and  $\varepsilon_r = 1/3.5, \sigma_r = 1/3$  for prolate ‘B’. In particular, these two cases have been found to demonstrate very interesting dynamics in direct numerical simulations [31]: For a prolate ‘A’ drop with  $(\varepsilon_r, \sigma_r) = (1, 1/3)$  addition of surfactant produces larger deformation than the clean drop case. Moreover, increasing surfactant coverage yields more pronounced drop deformation.

For small to moderate surfactant coverage, previous direct numerical simulations with finite Péclet number ( $Pe_s = 10$ ) [31] and spheroidal model with non-diffusive surfactant ( $Pe_s \rightarrow \infty$ ) [32] showed that increasing surfactant coverage gives rise to larger drop deformation regardless of electric field strength. This phenomenon is related to tip-stretching (for a detailed explanation see [32]), where the average surface tension is small and surfactant concentration gradient (and hence Marangoni stress) is large.

In contrast, for high surfactant coverage, the equilibrium drop deformation depends on the electric field strength [39]: the deformation, larger at low to moderate values of electric field strength compared to the clean drop case, is subsequently suppressed as the electric capillary number increases. This phenomenon is known as surface dilution. In this paper we focus on surfactant coverages  $\chi \leq 0.5$ , and on the range of electric capillary number  $Ca_E$  where tip-stretching is expected to dominate.

Figure 3(a) illustrates the excellent agreement in equilibrium deformation between the current model (solid curves),

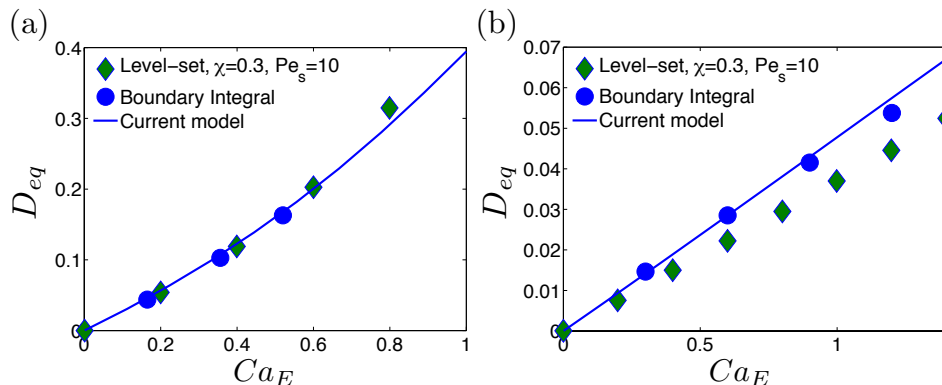


FIG. 3. Equilibrium deformation  $D_{eq}$  as a function of electric capillary number for a surfactant-laden, leaky dielectric drop. The electric parameters are (a) for a prolate ‘A’ (counterclockwise circulation) drop with  $\varepsilon_r = 1, \sigma_r = 1/3$ ; and (b) for a prolate ‘B’ (clockwise) drop with  $\varepsilon_r = 1/3.5, \sigma_r = 1/3$ . Symbols are from numerical simulations using a regularized level-set method [31] (green diamond), and a boundary integral equation method (blue circle) [35]; the current semi-analytical approach is represented by the solid line.

numerical simulations using regularized method (diamonds) [31] and boundary integral simulations (circles) [35]. Figure 3(b) shows the comparison between our model and numerical simulations for the prolate ‘B’ drop. While our predictions agree very well with boundary integral simulations, we observe some discrepancies with results from [31] as  $Ca_E$  increases. These discrepancies may be attributed to the weak inertial effect in the regularized level-set method [31], which is absent in the results by the boundary integral method and the current semi-analytical model. We note that, for prolate ‘A’ drops, the fluid stress combines with the electric stress to deform a drop along the direction of the electric field, while the opposite holds for prolate ‘B’ drops. We thus speculate that inertial effects (which influences the fluid stress [50, 51]) may cause the discrepancies observed in figure 3(b). Nevertheless, the overall relative errors between the boundary integral simulations and the current model are less than 10% in all cases studied.

#### IV. EFFECTS OF SURFACTANT TRANSPORT ON EQUILIBRIUM DEFORMATION

In this section we perform a systematic investigation of the effect of  $Pe_s$  on equilibrium drop deformation  $D_{eq}$ , exploring how surfactant transport and coverage combine to affect equilibrium drop shapes under a dc electric field.

##### A. Leaky dielectric drop

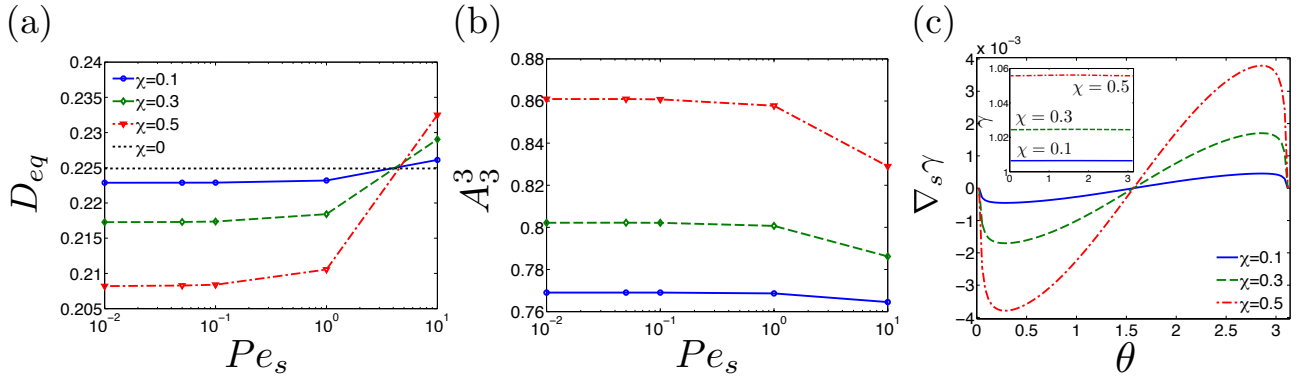


FIG. 4. Effects of Péclet number on the deformation number ( $D_{eq}$ ) and flow strength ( $A_3^3$ ) for a leaky dielectric prolate ‘A’ drop with  $\varepsilon_r = 1$ ,  $\sigma_r = 1/3$ . In (a)  $D_{eq}$  shows dependence on both surfactant coverage and  $Pe_s$ . For  $Pe_s \lesssim 5$ ,  $D_{eq}$  decreases with increasing  $\chi$ ; above that threshold, the opposite holds:  $D_{eq}$  increases with higher surfactant coverage. No such transition is observed in  $A_3^3$ . In (b),  $A_3^3$  monotonically decreases with increasing  $Pe_s$ , and higher surfactant coverage yields stronger flow. In (c) the Marangoni stress ( $\nabla_s \gamma$ ) and surface tension ( $\gamma$ , in inset) are plotted as a function of  $\theta = \cos^{-1}(\eta)$  for  $Pe_s = 0.1$ . The electric capillary number  $Ca_E = 0.67$

Figure 4 shows equilibrium drop deformation  $D_{eq}$  in panel (a) and flow strength  $A_3^3$  in panel (b) for a prolate ‘A’ leaky dielectric drop with  $Ca_E = 0.67$ . Panel (c) shows the Marangoni stress and surface tension (inset) at different values of  $\chi$  for  $Pe_s = 0.1$ . For small  $Pe_s$  (diffusion dominated regime) the equilibrium drop deformation  $D_{eq}$  decreases with surfactant coverage  $\chi$  while  $A_3^3$  increases with  $\chi$ . The corresponding dependencies of the Marangoni stress and surface tension are consistent with such trend: As  $\chi$  increases, both surface tension and Marangoni stress increase in magnitude, consistent with the decreasing trend of  $D_{eq}$  and the increasing trend of  $A_3^3$ . Our simulation results show that such trend in  $D_{eq}$  is reversed for  $Pe_s \geq 6$ :  $D_{eq}$  increases with  $\chi$  while  $A_3^3$  still increases with  $\chi$ . The dependence of equilibrium drop deformation on the surface Péclet number is also observed for a viscous drop under an external flow [52].

For  $Pe_s \gg 6$ , convection dominates; surfactant is swept, and accumulates, near the pole where it reduces the surface tension locally. In this process, known as tip stretching, the electric, hydrodynamic and Marangoni forces combine to deform the drop in the direction of the electric field. The deformation is consistent with previous works and experiments: it increases with  $\chi$ , and larger degree of deformation is accompanied with stronger convective transport. For large but finite Péclet numbers  $A_3^3$  decreases with increasing  $Pe_s$  but is not completely suppressed, unlike the case of non-diffusive surfactants ( $Pe_s \rightarrow \infty$ ) where the drop surface is completely immobilized by surfactants and the flow strength  $A_3^3 \rightarrow 0$  [32].

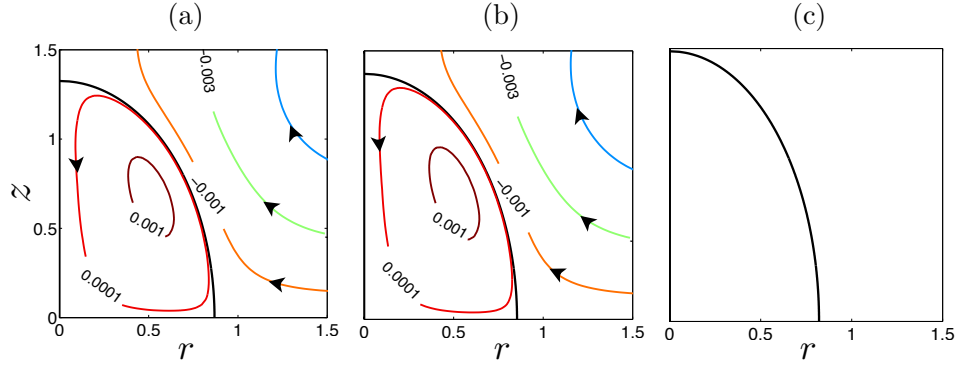


FIG. 5. Streamlines for the leaky dielectric prolate ‘A’ drop with  $\varepsilon_r = 1$ ,  $\sigma_r = 1/3$ , and  $\chi = 0.5$ : (a)  $Pe_s = 0.01$ ; (b)  $Pe_s = 10$ ; and (c)  $Pe_s \rightarrow \infty$  (the non-diffusive case from [32]). As the Péclet number  $Pe_s$  increases from (a) to (c), we observe larger deformation. In the non-diffusive limit the flow is completely suppressed as shown in (c).

Surfactants have a two-fold effect on drop electrohydrodynamics. On one end, for a given transport regime (fixed  $Pe_s$ ), the velocity field around a surfactant-covered drop is greatly reduced by surfactant coverage [31, 32]. On the other end, surfactant transport also affects drop electrohydrodynamics. In figure 5, we plot the streamlines for various values of Péclet number:  $Pe_s = 0.01$  (figure 5(a)),  $Pe_s = 10$  (figure 5(b)), and the non-diffusive case in [32] ( $Pe_s \rightarrow \infty$ , figure 5(c)). As  $Pe_s$  increases from (a) to (c), we observe increasing deformation and decreasing flow strength (consistent with  $A_3^3$  in figure 4(b)).

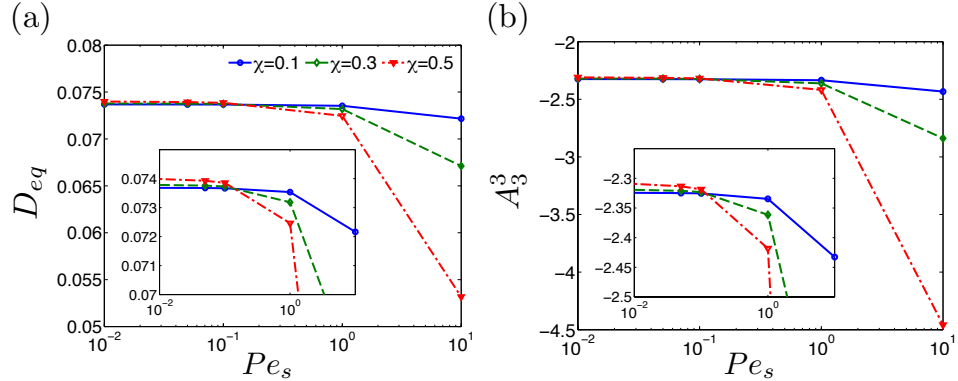


FIG. 6. Effects of Péclet number on the deformation number ( $D_{eq}$ ) and flow strength ( $A_3^3$ ) for a leaky dielectric prolate ‘B’ drop with  $\varepsilon_r = 1/3.5$ ,  $\sigma_r = 1/3$ . The transition from diffusion- to convection-dominated dynamics occurs around  $Pe_s \approx 10^{-1}$ . In the diffusion-dominated regime, higher surfactant coverage yields larger deformation (and stronger flow), though the difference between these is minimal. In the convection-dominated regime, we observe that  $D_{eq}$  decreases with  $Pe_s$  while the magnitude of flow strength ( $|A_3^3|$ ) increases with  $Pe_s$ . The electric capillary number  $Ca_E = 1.4$ .

Figures 6(a) and 6(b) show the equilibrium deformation  $D_{eq}$  and flow strength  $A_3^3$  for a leaky dielectric prolate ‘B’ drop with  $Ca_E = 1.4$ . For this prolate shape, increasing the surfactant coverage leads to equilibrium drop deformation smaller than a clean drop [31, 32] as captured by our model in figure 6(a) for  $Pe_s \gtrsim 0.1$ . For such a prolate ‘B’ drop the surfactant is swept from the pole to the equator, yielding smaller surface tension at the equator than at the poles. Thus, the deformation along the direction of the electric field (prolate ‘A’) is suppressed and the equilibrium drop shape is nearly spherical.

For diffusion-dominant surfactant transport ( $Pe_s < 0.1$ ),  $D_{eq}$  is nearly independent of surfactant coverage  $\chi$ . However, closer inspection (see insets in figure 6) reveals that higher surfactant coverage yields larger deformation. Dominated by diffusion, surfactants distribute evenly over the surface of the drop. Electric stresses that drive prolate ‘A’ shape result in slightly larger surfactant concentration near the poles, where the reduction in surface tension leads to higher deformation number. In this case, the smaller change in deformation number compared to the prolate ‘A’

case is ascribed to the clockwise circulation opposing deformation along the direction of the electric field.

The flow strength, represented by  $A_3^3$  in figure 6(b), varies with  $Pe_s$  in a similar fashion as drop deformation. Slightly stronger flow correlates with higher surfactant coverage for  $Pe_s < 0.1$ , and weaker flow dominates with lower surfactant concentration for  $Pe_s \gtrsim 0.1$ . Furthermore, the large magnitudes in figure 6(b) relative to figure 4(b) are consistent with stronger hydrodynamic stresses that are necessary to resist deformation along the direction of the electric field.

### B. Conducting drop

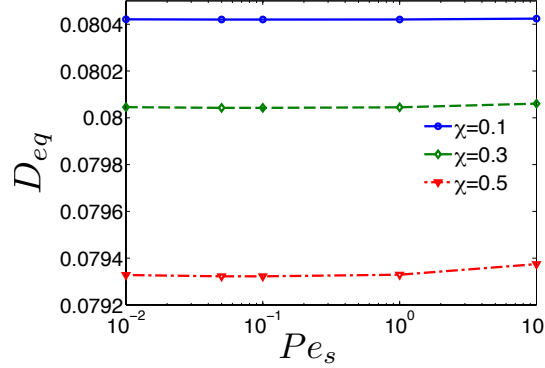


FIG. 7. Equilibrium deformation number as a function of Péclet number for a conducting drop. The effects of surfactant transport is shown for various values of surfactant coverage at  $Ca_E = 0.112$ . The electric parameters are  $\sigma_r = 10^{-3}$ ,  $\varepsilon_r = 1$ .

At steady equilibrium  $\partial\Gamma/\partial t = 0$  and  $\mathbf{u} \cdot \mathbf{n} = 0$ , thus we deduce from the surfactant transport equation (Eq. 10) that  $\mathbf{u}_s \Gamma \propto \nabla_s \Gamma$ . In the surfactant diffusion dominant regime, the surfactant distribution is rendered nearly uniform by strong diffusion, and thus  $\nabla_s \Gamma \approx 0$  and the tangential hydrodynamic stress also has to vanish at steady equilibrium. In the case of a conducting drop, there is no tangential Maxwell stress and therefore the flow strength ( $A_3^3$ ) depends only the average surfactant concentration gradient ( $f_{17}$  in Eq. 30). Thus we conclude that on a conducting drop, both the tangential velocity ( $\mathbf{u}_s \approx 0$ ) and the Marangoni stress ( $\nabla_s \gamma \approx 0$ ) vanish in the diffusion-dominant regime of surfactant transport. This implies that the conducting drop covered with surfactant is immobilized when the surfactant diffusion is strong. Moreover we expect the equilibrium deformation to be dependent on surfactant coverage and insensitive to Péclet number in the diffusion-dominant regime.

We consider the case of a prolate drop with  $\sigma_r = 10^{-3}$  and  $\varepsilon_r = 1$ . In figure 7, we plot the deformation number as a function of the Péclet. The result shows that surfactant transport does not seem to affect the dynamics of a conducting drop, and the deformation number is essentially independent of  $Pe_s$ . Moreover, increasing the surfactant coverage  $\chi$  yields smaller deformation, although the change in deformation from  $\chi = 0.1$  to  $\chi = 0.5$  is less than 2%. The inverse relation between surfactant coverage and drop deformation suggests the surface dilution dominates the surfactant dynamic for a conducting drop over a wide range of Péclet numbers. We also note that unlike leaky dielectric drops, there is no distinction between prolate ‘A’ and ‘B’ shapes, since tangential electric stresses are non-existent.

## V. EFFECTS OF SURFACTANT TRANSPORT ON TRANSIENT DYNAMIC

Studies of drops in electric field, and unsteady flow field ( $\partial\mathbf{u}/\partial t$ ) [8, 21] or surface charge relaxation  $\partial q/\partial t$  [21] revealed non-monotonic time evolution of the deformation. Time-dependent flow produces an overshoot in the unsteady deformation of the drop prior to reaching equilibrium, while  $\partial q/\partial t$ , characterized by the Saville number  $\mathcal{S}a$  [21], displays a shape transition at the early stage of transient deformation.

In the case of surfactant, the unsteady transport equation (Eq. 35) shows that the influence of  $\partial\Gamma/\partial t$  and  $\nabla_s \cdot (\Gamma \mathbf{u}_s)$  grows significantly with  $Pe_s$ . While the effects of surfactant convection on the equilibrium electro-deformation have been investigated [31, 32], changes in drop dynamics due to unsteady surfactant transport ( $\partial\Gamma/\partial t$ ) remain to be determined. Figure 8(a) shows the transient deformation of a leaky dielectric prolate ‘A’ drop under an electric field. We vary  $Pe_s \in [10, 20, 100]$  with  $Ca_E = 0.5$  and  $\chi = 0.3$ . As expected from §IV, the equilibrium deformation

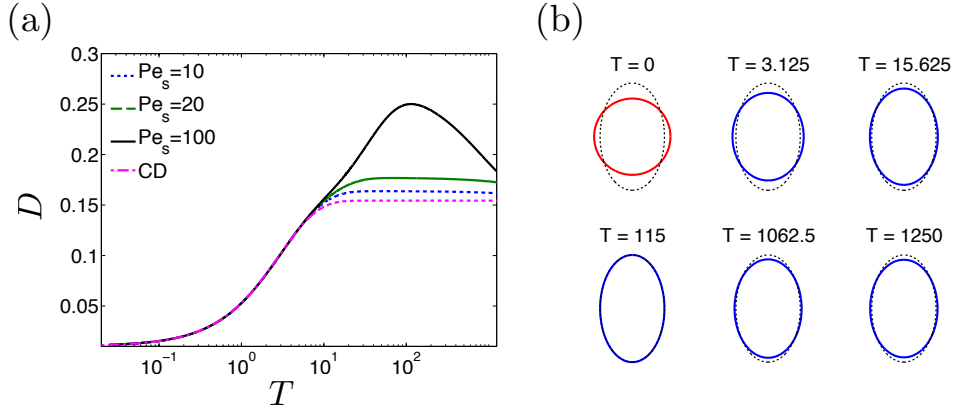


FIG. 8. (a) Deformation number  $D$  as a function of dimensionless time for a leaky dielectric drop with various values of  $Pe_s$ . The electric capillary number  $Ca_E = 0.5$  and surfactant coverage  $\chi = 0.3$ ; the electric parameters  $\varepsilon_r = 1$ ,  $\sigma_r = 1/3$ , corresponding to the prolate ‘A’ shape. The steady state curve for the clean drop case (CD) is denoted by the dotted line. (b) Snapshot of the drop shape at various times for  $D$  in (a) with  $Pe_s = 100$ . The dashed shape denotes the maximum shape achieved at peak overshoot.

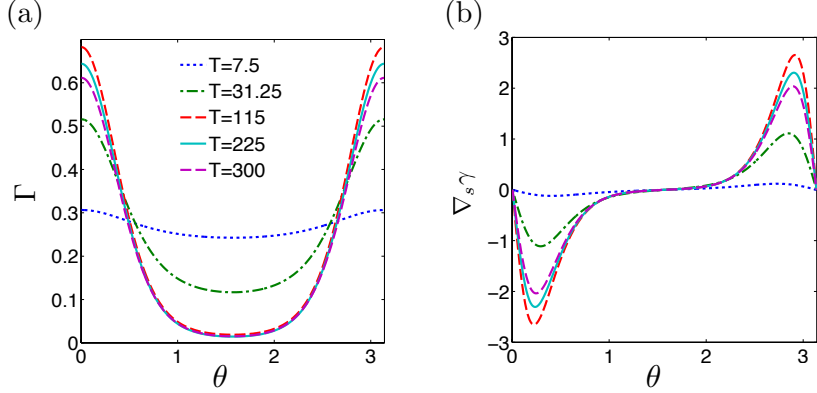


FIG. 9. The surfactant profile (a) and Marangoni stress (b) corresponding to  $Pe_s = 100$  in figure 8 are plotted as a function of  $\theta = \cos^{-1}(\eta)$ . Each curve denotes a fixed time, with the peak overshoot occurring at  $T \approx 115$ .

number depends on the surface Péclet number: stronger surfactant transport leads to larger deformation number. Furthermore, for these parameters, all curves display a transient overshoot, although negligible for  $Pe_s \leq 1$ . The feature becomes more pronounced for  $Pe_s > 1$ : it reaches around 1% of the equilibrium shape when  $Pe_s = 10$ , and around 36% when  $Pe_s = 100$ . In figure 8(b) we show snapshots of the drop shape at various times with  $Pe_s = 100$ . The dashed curve denotes the maximum deformed shape achieved by the drop, at the peak of the overshoot. The maximum shape is reached around  $T \approx 115$ . From that point, the drop shape settles to its equilibrium.

Figure 9 shows the corresponding distributions of surfactant concentration (figure 9(a)) and Marangoni stress (figure 9(b)) as a function of the surface parameter  $\theta = \arccos(\eta)$  at various time instances. Transient overshoots of surfactant concentration and Marangoni stress near the poles are observed at  $T \approx 115$ . However, the causal relationship of these correlations with the transient overshoot in deformation is not obvious and will be investigated in the future; here we only report these correlations.

The deformation of a leaky dielectric drop under an electric field is the result of induced (creeping) flow caused by tangential Maxwell stresses. However, these tangential stresses do not exist in perfectly conducting drops. We ran simulations for the perfectly conducting drop (keeping all parameters unchanged from the prolate ‘A’ case in figure 8) and observed only monotonic behaviors of the unsteady deformation, suggesting the importance of tangential flows in leaky dielectric drops and the transient overshoot due to surfactant.

## VI. CONCLUSION

We investigate the effect of surfactant transport on the electro-deformation of a viscous drop under a DC electric field. Extending previous work on non-diffusive surfactant [32] here we focus on two surfactant transport regimes characterized by the surface Péclet number ( $Pe_s$ ). The advantage of our modal approach over direct numerical simulations is that we can identify salient features of surfactant-laden drop electrodynamics by efficiently examining the deformation dynamics for different combinations of parameter values. We derived analytical equations describing the electro-deformation of surfactant-laden leaky dielectric and conducting drops (both clean and surfactant-laden) in the presence of insoluble surfactants. We validate our model by comparing against published results from both experiments and numerical simulations, and found good agreement for the clean conducting drops [6, 48], and the surfactant-laden drops [31]. We then perform a systematic study of the effects of surfactant transport on the equilibrium drop deformation.

In this study we focus on two modes of prolate deformation: one with counter-clockwise circulation ('A'), and another with clockwise circulation ('B'). Depending on the surfactant transport regime, we observe different behaviors of deformation for leaky dielectric drops: when surfactant diffusion dominates ( $Pe_s \ll 1$ ), prolate 'A' ('B') yields smaller (larger) equilibrium deformation with increasing surfactant coverage, compared to a clean drop. On the other hand, when convection dominates ( $Pe_s \gg 1$ ), the equilibrium drop deformation increases (decreases) with larger surfactant coverage on a prolate 'A' ('B') drop. We also contrast leaky dielectric versus conducting drops in Appendix C. For a prolate 'A' drop we find consistently larger equilibrium drop deformation for a leaky dielectric drop compared to a conducting drop, while for prolate 'B' we identify cases where larger deformation is found for a conducting drop compared to a leaky dielectric drop. Finally, we study the effect of the surfactant transport on the evolution of drop shape. We found the drop undergoes an overshoot in the early deformation phase, before settling to its equilibrium shape – a dynamic similar to the overshoot observed for electrohydrodynamic governed by the unsteady Stokes equation [21].

Another important aspect of surfactant-laden drop electrohydrodynamics is surfactant solubility, known to lead to drastically different drop dynamics in the absence of an external electric field [43]. Recent experiments with soluble surfactants have revealed rich dynamics of drops electrohydrodynamics under a strong electric field [53]. Future theoretical investigations will attempt to provide insights into how surfactant solubility and electrohydrodynamics may combine to affect the drop deformation and dynamics. Specifically, we ponder whether the flow is still suppressed when sorption kinetics are accounted for, or if surfactant solubility can be used to control the electro-deformation of drops, and/or alter the dynamics in the various transport regimes. We are now expanding our model to incorporate the exchange of surfactant between the drop surface and the bulk under an electric field.

Finally, we remark that charge relaxation, which is not accounted for in this work, may become important for systems with small drops or large interfacial surface. It has been shown recently that finite charge relaxation can lead to interesting dynamics for clean drops [21]. Its influences on the transient behavior of surfactant-laden drops may be more prominent when the drop is undergoing extreme deformation such as breakup.

### Appendix A: Integrals in the prolate spheroidal model

The functions  $f_{11}(\xi_0) - f_{15}(\xi_0)$  in Eq. 25 are given by

$$f_{11} = \int \frac{\eta G_3(\eta)}{\xi_0^2 - \eta^2} d\eta, \quad (\text{A1})$$

$$f_{12} = \frac{1}{\xi_0^2 - 1} \int G_3(\eta) \left[ \frac{2\eta G'_3(\eta)}{(\xi_0^2 - \eta^2)^2} + \frac{G''_3(\eta)}{\xi_0^2 - \eta^2} \right] d\eta, \quad (\text{A2})$$

$$f_{13} = \frac{G'_3 G''_5 - G'_5 G''_3}{2N} f_{11}, \quad (\text{A3})$$

$$f_{14} = -\xi_0 H'_3 \int \frac{\eta G_3(\eta)}{(\xi_0^2 - \eta^2)^2} d\eta + \frac{H''_3}{2} f_{11}, \quad (\text{A4})$$

$$f_{15} = \xi_0 H'_3 \int \frac{\eta G_3(\eta)}{(\xi_0^2 - \eta^2)^2} d\eta - \frac{(G_3 G''_5 - G_5 G''_3) H'_3}{2N} f_{11}, \quad (\text{A5})$$

$$f_{17} = \frac{1}{\sqrt{\xi_0^2 - 1}} \int_{-1}^1 \frac{G_3(\eta) \Gamma'(\eta)}{\sqrt{\xi_0^2 - \eta^2} (1 - \chi \Gamma)} d\eta. \quad (\text{A6})$$



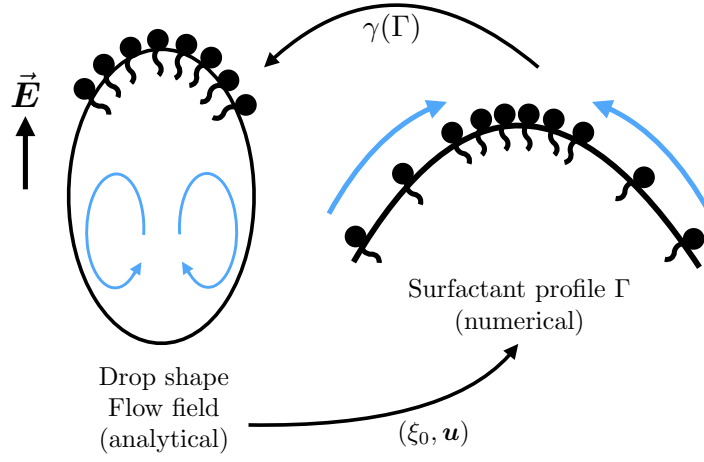


FIG. 10. The semi-analytical algorithm: At  $t_n$  the drop shape  $\xi_0$  and flow field  $\mathbf{u}$  is computed using the large deformation spheroidal analysis. This information is then used as input to the surfactant transport, in order to determine the surfactant profile  $\Gamma$  numerically with a collocation method. With the surfactant concentration at hand, we determine the change in surface tension, the drop shape and the flow field at time  $t_{n+1}$ . This process is repeated until a steady-state is reached.

Furthermore, the functions  $f_{21}(\xi_0) - f_{26}(\xi_0)$  in Eq. 25 and Eq. 31 are given by

$$f_{21} = \frac{\xi_0^2}{2} \int \frac{(3\eta^2 - 1)(\eta^2 - 1)}{\xi_0^2 - \eta^2} d\eta, \quad (\text{A7})$$

$$f_{22} = -H'_3 \int \frac{(1 - 3\eta^2)(2\eta^4 + \xi_0^2 - 3\xi_0^2\eta^2)}{(\xi_0^2 - \eta^2)^2} d\eta + 3H_3\xi_0 \int \frac{1 - 3\eta^2}{\xi_0^2 - \eta^2} d\eta, \quad (\text{A8})$$

$$f_{23} = -\frac{49}{30N} G_3 H'_3 (1 - 3\xi_0^2) + H'_3 \int \frac{(1 - 3\eta^2)(2\eta^4 + \xi_0^2 - 3\xi_0^2\eta^2)}{(\xi_0^2 - \eta^2)^2} d\eta, \quad (\text{A9})$$

$$f_{24} = \frac{1}{c} \left[ \xi_0 (\xi_0^2 - 1)^{1/2} \int \frac{\gamma (3\eta^2 - 1)}{(\xi_0^2 - \eta^2)^{3/2}} d\eta + \frac{\xi_0}{(\xi_0^2 - 1)^{1/2}} \int \frac{\gamma (3\eta^2 - 1)}{(\xi_0^2 - \eta^2)^{1/2}} d\eta \right], \quad (\text{A10})$$

$$f_{25} = -\frac{\xi_0}{\xi_0^2 - 1} \int \frac{(1 - 3\eta^2)(2\xi_0^2 - \eta^2 - 1)G'_3(\eta)}{(\xi_0^2 - \eta^2)^2} d\eta + 3\xi_0 \int \frac{1 - 3\eta^2}{\xi_0^2 - \eta^2} d\eta - \frac{(\mu_r - 1)f_{12} + f_{13}}{\mu_r f_{14} + f_{15}} f_{22}, \quad (\text{A11})$$

$$f_{26} = \frac{\xi_0}{\xi_0^2 - 1} \int \frac{(1 - 3\eta^2)(2\xi_0^2 - \eta^2 - 1)G'_3(\eta)}{(\xi_0^2 - \eta^2)^2} d\eta - \frac{49}{30N} (1 - 3\xi_0^2) G'_3 - \frac{(\mu_r - 1)f_{12} + f_{13}}{\mu_r f_{14} + f_{15}} f_{23}. \quad (\text{A12})$$

$\gamma$  is the dimensionless surface tension given by Eq. 34, and  $N = G_3 G'_5 - G_5 G'_3$ .

## Appendix B: Numerical algorithm details

### 1. Model limitations

We made some assumptions in order to arrive at the shape equations 25 and 31. Here we discuss how these assumptions affect predictions using our model. First, based on experimental findings, we assume the drop remains spheroidal in shape. However, other subtle shape variations may be at play during the drop dynamics, and these may account for discrepancies in the electro-deformation at moderate to high values of electric capillary number. Second, only the first spheroidal harmonics mode is considered in this study. The truncation error, coupled with averaging the stress balances, influences the flow circulation and, by extension, surfactant dynamics.



Moreover, for a surfactant-covered drop, once the surfactant concentration reaches the maximum packing at a location on the drop surface, the fluid flow and the interface deformation there conspire to immobilize the drop surface so that no more surfactant can flux into that location [39, 54–56]. Such suppression of interfacial flow can only be approximated in our modal analysis with a single mode.

## 2. Numerical implementation

The steps we take to simulate the dynamic of a surfactant-laden drop in an electric field are illustrated in figure 10. At time  $t_n$ , the governing equation for the drop shape  $\xi_0$  and the surfactant transport equation are solved numerically using various algorithms. The integrals involving the Marangoni stress ( $f_{17}$ ) and the surface tension ( $f_{24}$ ) are resolved by Gauss-Legendre quadrature with  $n$  nodes that are used to discretize the drop spatial distribution  $\eta$ . We then use the integrals to solve the ordinary differential Eq. 25 and Eq. 31 using a fourth-order Runge-Kutta method. Once the drop shape, and consequently the flow field, are obtained, the information is used to obtain the surfactant distribution profile. The surfactant concentration  $\Gamma$  is obtained by solving the transport equation (Eq. 36). This is a nonlinear equation that does not admit analytical solutions, except in special limits [32, 57]. To consider the full range of Péclet number, we treat the surfactant transport as a boundary value problem and solve the equation using MATLAB's built-in *bvp4c* function, a finite difference code that implements the three-stage Lobatto IIIa collocation method [58]. The boundary value problem is set up as a system of two ordinary differential equations with variables  $y_1 = \Gamma$  for the surfactant concentration and  $y_2 = d\Gamma/d\eta$ . Surfactant conservation is enforced by augmenting the system  $\{y_1, y_2\}$  with a third variable  $y_3 \equiv \int_{-1}^1 \Gamma h_\eta h_\zeta d\eta$ , with boundary condition  $y_3(1) = \text{total amount of surfactant}$ . Once the surfactant concentration  $\Gamma$  is obtained, we determine the change in the surface tension  $\gamma$ , and feed the result back into Eq. 25 and Eq. 31 to determine the drop shapes and flow fields at the next time step  $t_{n+1}$ . This process is repeated until either a steady-state is reached, when the change in successive  $\xi_0$  iterates  $|\Delta\xi_0| \leq 10^{-6}$ , or the simulation stops, signaling that a spheroidal shape is not attainable.

## Appendix C: Comparison between Leaky Dielectric and Conducting Drops

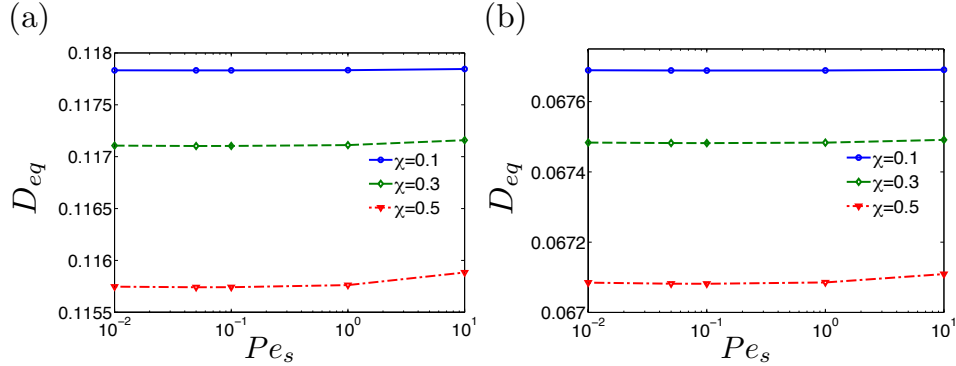


FIG. 11. Effects of Péclet number on the deformation number ( $D_{eq}$ ) for (a) a conducting prolate ‘A’ drop with  $\varepsilon_r = 1$ ,  $\sigma_r = 1/3$  and  $Ca_E = 0.67$ , and (b) a conducting prolate ‘B’ drop with  $\varepsilon_r = 1/3.5$ ,  $\sigma_r = 1/3$  and  $Ca_E = 1.4$ . In both cases the deformation remains relatively constant across  $Pe_s \lesssim 1$ , then shows small increases as convection starts dominating. Moreover, higher surfactant coverage yields smaller deformation.

To facilitate comparison with the leaky dielectric drop in the previous section, we now consider the leaky drop with  $\sigma_r = 1/3$ . We note this is strictly for comparison purpose since for a conducting drop it is necessary  $\sigma_r \ll 1$ . However, we point out that even in this case, the dependence of the deformation number on surfactant transport and surfactant coverage is qualitatively the same. Figure 11(a) shows the deformation number for a prolate ‘A’ conducting drop with  $Ca_E = 0.67$ , while figure 11(b) shows the deformation number for a prolate ‘B’ conducting drop with  $Ca_E = 1.4$ . Here as well, as shown in figure 11(a), deformation remains independent of  $Pe_s$ . Also, the change in deformation between  $\chi = 0.1$  and  $\chi = 0.5$  is less than 2%.

The importance of electric tangential stresses and the induced flow in surfactant transport is evident when we contrast the flow strength  $A_3^3$  for leaky dielectric drops (of order  $10^{-1}$  [figure 4(b)]), to a vanishingly small flow

strength  $A_3^3$  in conducting drops. The deformation in figure 11(b) for a prolate ‘B’ drop is also independent of  $Pe_s$ , with an increase in the surfactant coverage yielding a negligible enhancement in deformation. We attribute the similarities between figures 11(a) and 11(b) to the lack of tangential flows in a conducting viscous drop.

When contrasting leaky dielectric and conducting drops, both laden with insoluble surfactant with  $Pe_s \gg 1$ , we generally expect a leaky dielectric drop would undergo larger deformation than a conducting drop (see figure 6(a) versus figure 11(b)). This is because the additional tangential flows in leaky dielectric drops contribute significantly to overall deformation. However, we found that when conditions are such that moderate surfactant concentration is combined with strong convection and clockwise flow circulation, conducting drops can actually yield larger deformation than a leaky dielectric drop at equilibrium. Closer analysis of figures 6(a) and 11(b) reveals that for  $Pe_s = 10$ ,  $D_{eq} = 0.0532$  for a leaky dielectric drop, while  $D_{eq} = 0.0671$  for a conducting drop, or 26% larger. Note that while the change in deformation is significant, it may prove difficult to observe in experiments since  $D_{eq}$  is of order  $10^{-2}$ . For experimental validation, it is more helpful to compare the flow field via  $A_3^3$  with clear variations in order of magnitude. Indeed, for a prolate ‘B’ leaky dielectric drop  $A_3^3 \approx -4.5$  [figure 6(b)] compared to a vanishingly small  $A_3^3$  for a conducting drop.

## ACKNOWLEDGMENTS

H. Nganguia thanks K. Pietrzyk for helpful discussions about the analytical derivations, and C. Sorgentone for helpful discussions and the boundary integral numerical simulations used to validate the proposed semi-analytical method. Y.-N. Young was partially supported by NSF under grants DMS-1412789 and DMS-1614863, and by the Flatiron Institute, a division of the Simons Foundation.

- 
- [1] C. T. O’Konski and H. C. Thacher, *J. Chem. Phys.* **57**, 955 (1953).
  - [2] R. S. Allan and S. G. Mason, *Proc. R. Soc. Lond. A* **267**, 45 (1962).
  - [3] G. Taylor, *Proc. R. Soc. Lond. A* **291**, 159 (1966).
  - [4] J. R. Melcher and G. I. Taylor, *Annu. Rev. Fluid Mech.* **1**, 111 (1969).
  - [5] D. A. Saville, *Annu. Rev. Fluid Mech.* **29**, 27 (1997).
  - [6] J.-W. Ha and S.-M. Yang, *J. Fluid Mech.* **405**, 131 (2000).
  - [7] E. K. Zholkovskij, J. H. Masliyah, and J. Czarnecki, *J. Fluid Mech.* **472**, 1 (2002).
  - [8] G. Supeene, C. R. Koch, and S. Bhattacharjee, *J. Colloid Int. Sci.* **318**, 463 (2008).
  - [9] J.-W. Ha and S.-M. Yang, *Phys. Fluids* **12**, 764 (2000).
  - [10] E. Lac and G. M. Homsy, *J. Fluid Mech.* **590**, 239 (2007).
  - [11] N. Benteitis and S. Krause, *Langmuir* **21**, 6194 (2005).
  - [12] M. Zabaranin, *SIAM J. Appl. Math.* **73**, 677 (2013).
  - [13] M. Zabaranin, *SIAM J. Appl. Math.* **76**, 1606 (2016).
  - [14] P. R. Brazier-Smith, *Phys. Fluids* **14**, 1 (1971).
  - [15] P. R. Brazier-Smith, S. G. Jennings, and J. Latham, *Proc. R. Soc. Lond. A* **325**, 363 (1971).
  - [16] M. Miksis, *Phys. Fluids* **24**, 1967 (1981).
  - [17] O. A. Basaran and L. E. Scriven, *Phys. Fluids* **1**, 799 (1989).
  - [18] H. Nganguia, Y.-N. Young, A. T. Layton, W.-F. Hu, and M.-C. Lai, *Commun. Comput. Phys.* **18**, 429 (2015).
  - [19] W.-F. Hu, M.-C. Lai, and Y.-N. Young, *J. Comp. Phys.* **282**, 47 (2014).
  - [20] G. I. Taylor, in *Proc. 11th Intl. Cong. Theor. App. Mech. (Munich 1964)* (Springer Verlag, Heidelberg, 1964) pp. 790–796.
  - [21] J. A. Lanauze, L. M. Walker, and A. S. Khair, *Phys. Fluids* **25**, 112101 (2013).
  - [22] J. A. Lanauze, L. M. Walker, and A. S. Khair, *J. Fluid Mech.* **774**, 245 (2015).
  - [23] D. Das and D. Saintillan, *J. Fluid Mech.* **810**, 225 (2017).
  - [24] J. Q. Feng, *Proc. R. Soc. Lond. A* **455**, 2245 (1999).
  - [25] H. Nganguia, Y.-N. Young, A. T. Layton, M.-C. Lai, and W.-F. Hu, *Phys. Rev. E* **93**, 053114 (2016).
  - [26] H. A. Stone and L. G. Leal, *J. Fluid Mech.* **220**, 161 (1990).
  - [27] P. M. Vlahovska, *Phys. Rev. Fluids* **1**, 060504 (2016).
  - [28] S. Takagi and Y. Matsumoto, *Annu. Rev. Fluid Mech.* **43**, 615 (2011).
  - [29] J.-W. Ha and S.-M. Yang, *J. Colloid Int. Sci.* **175**, 369 (1995).
  - [30] J.-W. Ha and S.-M. Yang, *J. Colloid Int. Sci.* **206**, 195 (1998).
  - [31] K. E. Teigen and S. T. Munkejord, *Phys. Fluids* **22**, 112104 (2010).
  - [32] H. Nganguia, Y.-N. Young, P. M. Vlahovska, J. Bławdziewicz, J. Zhang, and H. Lin, *Phys. Fluids* **25**, 092106 (2013).
  - [33] N. Dubash and A. J. Mertel, *J. Fluid Mech.* **581**, 469 (2007).
  - [34] J. Zhang, J. D. Zahn, and H. Lin, *Phys. Rev. E* **87**, 043008 (2013).
  - [35] C. Sorgentone, A.-K. Tornberg, and P. Vlahovska, *J. Comput. Phys.* **389**, 111 (2019).
  - [36] G. Dassios, M. Hadjinicolaou, F. A. Coutelieres, and A. C. Payatakes, *Int. J. Engng Sci.* **33**, 1465 (1995).

- [37] N. Dubash and A. J. Mertel, Phys. Fluids **19**, 072101 (2007).
- [38] N. Dubash and A. J. Mertel, Phys. Fluids **19**, 073104 (2007).
- [39] Y. Pawar and K. J. Stebe, Phys. Fluids **8** (7), 1738 (1996).
- [40] C. D. Eggleton, T.-M. Tsai, and K. J. Stebe, Phys. Rev. Lett. **87**, 048302 (2001).
- [41] M. R. Booty and M. Siegel, J. Fluid Mech. **544**, 243 (2005).
- [42] M. Hameed, M. Siegel, Y.-N. Young, J. Li, M. R. Booty, and D. T. Papageorgiou, J. Fluid Mech. **594**, 307 (2008).
- [43] Y.-N. Young, M. R. Booty, M. Siegel, and J. Li, Phys. Fluids **21**, 072105 (2009).
- [44] P. F. Salipante and P. M. Vlahovska, Phys. Fluids **22**, 112110 (2010).
- [45] M. Ouriemi and P. M. Vlahovska, J. Fluid Mech. **751**, 106 (2014).
- [46] V. Vivacqua, S. Mhatre, M. Ghadiri, A. M. Abdullah, A. Hassanpour, M. J. Al-Marri, B. Azzopardi, B. Hewakandamby, and B. Kermani, Chem. Eng. Res. Des. **104**, 658 (2015).
- [47] A. Balakrishnan, B. D. Rege, G. L. Amidon, and J. E. Polli, J. Pharm. Sci. **93**, 2064 (2004).
- [48] R. B. Karyappa, S. D. Deshmukh, and R. M. Thaokar, J. Fluid Mech. **754**, 550 (2014).
- [49] O. O. Ajayi, Proc. R. Soc. Lond. A **364**, 499 (1978).
- [50] L. G. Leal, Ann. Rev. Fluid Mech. **12**, 435 (1980).
- [51] Y. Y. Renardy and V. Cristini, Phys. Fluids **13**, 7 (2001).
- [52] W. J. Milliken, H. A. Stone, and L. G. Leal, Phys. Fluids **5** (1), 69 (1993).
- [53] J. A. Lanauze, R. Sengupta, B. J. Bleier, B. A. Yezer, A. S. Khair, and L. M. Walker, Soft Matter **14**, 9351 (2018).
- [54] C. D. Eggleton, Y. P. Pawar, and K. J. Stebe, J. Fluid Mech. **385**, 79 (1999).
- [55] C. D. Eggleton and K. J. Stebe, J. Coll. Int. Sci. **208**, 68 (1998).
- [56] Y. Wang, D. Papageorgiou, and C. Maldarelli, J. Fluid Mech. **390**, 251 (1999).
- [57] C. Kallendorf, A. Fath, M. Oberlack, and Y. Wang, Phys. Fluids **27**, 082104 (2015).
- [58] *MATLAB version 8.3.0.532 (R2014a)*, The Mathworks, Inc., Natick, Massachusetts (2014).